GEOPHYSICS, VOL. 49, NO. 11 (NOVEMBER 1984); P. 1933–1957, 15 FIGS., 1 TABLE.

SH-wave propagation in heterogeneous media: Velocity-stress finite-difference method

Jean Virieux*

ABSTRACT

A new finite-difference (FD) method is presented for modeling *SH*-wave propagation in a generally heterogeneous medium. This method uses both velocity and stress in a discrete grid. Density and shear modulus are similarly discretized, avoiding any spatial smoothing. Therefore, boundaries will be correctly modeled under an implicit formulation. Standard problems (quarter-plane propagation, sedimentary basin propagation) are studied to compare this method with other methods. Finally a more complex example (a salt dome inside a two-layered medium) shows the effect of lateral propagation on seismograms recorded at the surface. A corner wave, always in-phase with the incident wave, and a head wave will appear, which will pose severe problems of interpretation with the usual vertical migration methods.

INTRODUCTION

Propagation in heterogeneous media has focused the attention of seismologists for the last ten years. Analysis of effects of topography and internal interfaces concentrates a wide range of analytical and numerical tools. Direct time and space discretization leads to finite-difference (Alterman and Karal, 1968; Boore, 1972; Alford et al., 1974) and finite-element (Smith, 1975) methods. Spectral decomposition leads to different methods depending upon how the space dependence is handled. Transforming to the horizontal wavenumber domain, discretizing, and truncating it leads to the Aki-Larner method (Aki and Larner, 1970), in which the scattered field is described as a linear combination of plane waves having discrete horizontal wavenumbers. By a boundary integral equation approach in the space domain, a complete representation of the scattered field can be obtained along boundaries. Coefficients are determined by a least-squares method, after discretizing the boundaries (Sanchez-Sesma and Esquivel, 1979). An alternative to the full-wave methods described above are the asymptotic techniques known generally as ray theory (Červeny et al., 1977). For laterally heterogeneous methods, glorified optics was proposed by Hong and Helmberger (1978), who took into account the curvature of the wavefront at interfaces of a 2-D medium, while Lee and Langston (1983) handled the 3-D case by introducing two curvatures called principal curvatures.

In this paper, I focus attention on wave propagation solved by finite-difference (FD) methods. Two formulations can be distinguished, as pointed out by Kelly et al. (1976). The homogeneous approach solves the propagation equation in each homogeneous medium, and it verifies explicit boundary conditions between the different media. The heterogeneous formulation, on the other hand, directly solves the propagation equation in a heterogeneous medium where physical properties are spatially variable. Therefore, boundary conditions are satisfied implicitly.

In the standard formulation of the second-order partial differential equation, only displacement is calculated at each node of the finite-difference grid. In the homogeneous formulation, the boundary conditions, which are the continuity of displacement and the stress at the interface, are solved explicitly. This method gives an infinite weight to displacements (that is also required by wave-equation discretization) and also an infinite weight to stress (that is not implied by wave-equation discretization). Different approximations of the derivatives at the interfaces lead to different orders of accuracy at the boundaries. Kummer and Behle (1982) summarized most of the work done since Alterman and Karal (1968). Because this paper deals with the heterogeneous formulation, I refer to them for a review of the homogeneous approach.

In the heterogeneous formulation discontinuities are replaced by numerical transition zones in which elastic parameter gradients are bounded (Kelly et al., 1976). Another approach by Tikhonov and Samarskii (see references in Mitchell, 1969, p. 23), discussed by Boore (1972), reduces this smoothing to a grid size by introducing a new variable, which is equivalent to stress (discussed below).

In this paper, I propose to apply an FD scheme that includes both velocity and stress in the equations of motion. This method was used by Madariaga (1976) and Virieux and Ma-

Manuscript received by the Editor March 21, 1984; revised manuscript received May 21, 1984.
*Formerly Department de Geotectonique, Universite Pierre et Marie Curie, Paris; presently Laboratoire de Sismologie, Institut de Physique du Globe de Paris, Universite Paris VII, 4, place Jussieu-T 24, 4eme etage, 75005 Paris, France.

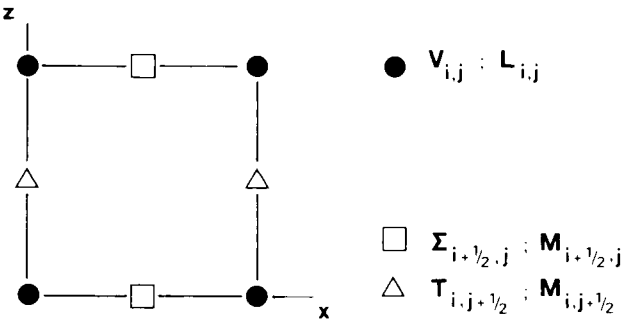

FIG. 1. Discretization of the medium on a staggered grid. Black symbols are for velocities and lightness at time kdt. White symbols are for stresses and shear modulus at time $[k + 1/2]dt$.

dariaga (1982) to solve crack problems. It was reviewed in Aki and Richards (1980, Chap. 14). I formulate the problem: equations, initial and boundary conditions, and its numerical formulation. The quarter-plane problem will be studied to demonstrate the validity of the numerical method by comparison with analytical solutions, although its validity already was established by previous work on crack problems. The somewhat canonical problem of sedimentary basin excitation by an incident vertical plane wave will be studied for comparison with other techniques; this study appears to be a difficult configuration for FD modeling. Finally, the FD method is applied to study a salt dome in a two-layered medium. The interpretation of seismograms at the surface will be discussed, emphasizing the importance of lateral wave propagation. I conclude with an analysis of the possibilities of this method and with the importance of image representation for the interpretation.

PROBLEM FORMULATION

Equations

I begin by presenting two-dimensional SH-wave propagation in a heterogeneous medium. Velocity and density are functions of x and z. The horizontal displacement v along the y-axis satisfies the scalar wave equation:

$$\rho(x, z)\frac{\partial^2 v}{\delta t^2} = \frac{\delta}{\delta x}\left[\mu(x, z)\frac{\delta v}{\delta x}\right] + \frac{\delta}{\delta z}\left[\mu(x, z)\frac{\delta v}{\delta z}\right], \qquad (1)$$

where $\rho(x, z)$ is the density and $\mu(x. z)$ the shear modulus at a point $M(x, z)$ of the medium. Instead of using this second-order hyperbolic equation, we go back to the original elastodynamic equations, reintroducing shear stresses σ_{xy} and σ_{zy}, i.e.,

$$\rho(x, z)\frac{\delta^2 v}{\delta t^2} = \frac{\delta}{\delta x}(\sigma_{xy}) + \frac{\delta}{\delta z}(\sigma_{zy}), \qquad \text{(equation of motion)}$$

$$\left.\begin{aligned} \sigma_{xy} &= \mu(x, z)\frac{\delta v}{\delta x}, \\ \text{and} \qquad & \\ \sigma_{zy} &= \mu(x, z)\frac{\delta v}{\delta z}. \end{aligned}\right\} \qquad \text{(Hooke's laws)} \qquad (2)$$

This system is transformed into a first-order hyperbolic system which states

$$\frac{\delta \dot{v}}{\delta t} = \ell(x, z)\left[\frac{\delta}{\delta x}(\sigma_{xy}) + \frac{\delta}{\delta z}(\sigma_{zy})\right],$$

$$\frac{\delta}{\delta t}\sigma_{xy} = \mu(x, z)\frac{\delta \dot{v}}{\delta x}, \qquad (3)$$

and

$$\frac{\delta}{\delta t}\sigma_{zy} = \mu(x, z)\frac{\delta \dot{v}}{\delta z},$$

where $\ell(x, z)$ is the inverse of density: the lightness or the buoyancy. Dots note a time derivative. System (3) propagates explicitly, velocity and stress inside the medium.

I compare this formulation with the method of Tikhonov and Samarskii (see Mitchell, 1969, p. 23). The introduction of auxiliary variables in their method requires averaging the shear modulus over a grid mesh, so that the discretization of density and shear modulus is quite different. My equations, on the other hand, maintain a certain symmetry between velocity and stress so that density (or lightness) and shear modulus are concentrated at the nodes, as usual in an FD formulation.

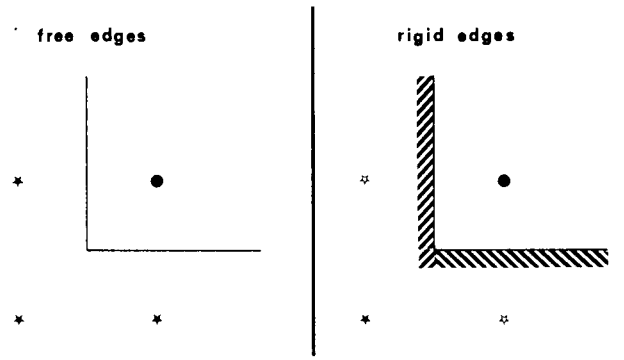

FIG. 2. Quarter-plane geometry: Image theory interpretation for free edges (left) and for rigid edges (right).

Initial conditions

The medium is supposed to be in equilibrium at time $t = 0$, i.e., stress and velocity are set to zero everywhere in the medium. Because of these initial conditions, propagating stress and velocity is also equivalent to propagating "time-integrated stress" and displacement.

Boundary conditions

Internal interfaces are not treated by explicit boundary conditions because they are represented naturally by changes of the elastic parameters and density. Only five explicit boundary conditions are required: source excitation, and the four edges of the finite-sized vertical grid. Depending upon the problem, different boundary conditions can be used on the edges: approximate-radiation conditions (for simulating an infinite

medium), stress-free conditions (also known as Neumann condition or free-surface), or zero-velocity conditions equivalent to zero-displacement conditions (Dirichlet condition or rigid-surface). The radiation conditions are equivalent to the condition B-1 of Clayton and Engquist (1980), and correspond to plane-wave radiation conditions.

Source excitation is solved by using the approach of Alterman and Karal (1968). For any kind of source, the excitation is applied to velocity. Incident velocity and residual velocity are both considered along a line around the source. The known incident velocity is applied outwardly from this line, while the source zone inside this line is transparent for the residual velocity coming from reflection, refraction, and diffraction of the incident velocity field. In our illustrative examples, two basic sources will be presented: the impulsive point source, and the impinging plane wave.

For an implusive point source, the incident velocity is obtained by convolving the infinite-medium Green's function with the source excitation as proposed by Alford et al. (1974). The convolution is obtained in the time domain instead of the frequency domain. The impulsive excitation will be

$$f(t) = (t - t_0)e^{-\alpha(t-t_0)^2},$$

where α controls the wavelength content of the excitation. α is 1 000 and t_0 is 0.2 s in the computations.

For plane-wave excitation, the incident velocity is given by a Ricker wavelet as

$$f(t) = \frac{\pi}{2}(a - \tfrac{1}{2})e^{-a},$$

where $a = \pi(t - t_s)^2/t_p^2$. In these computations, t_s is 20 s and t_p is 18.3 s.

NUMERICAL SIMULATION

Derivatives are discretized using centered finite-differences. Discretization of equations leads to a unique staggered grid, as shown in Figure 1. The numerical scheme, equivalent to system (3), is as follows:

$$V_{i,j}^{k+1/2} = V_{i,j}^{k-1/2} + \frac{dt}{dx} L_{i,j}[\Sigma_{i+1/2,j}^{k} - \Sigma_{i-1/2,j}^{k}] + \frac{dt}{dz} L_{i,j}[T_{i,j+1/2}^{k} - T_{i,j-1/2}^{k}],$$

$$\Sigma_{i+1/2,j}^{k+1} = \Sigma_{i+1/2,j}^{k} + \frac{dt}{dx} M_{i+1/2,j}[V_{i+1,j}^{k+1/2} - V_{i,j}^{k+1/2}], \quad (4)$$

and

$$T_{i,j+1/2}^{k+1} = T_{i,j+1/2}^{k} + \frac{dt}{dz} M_{i,j+1/2}[V_{i,j+1}^{k+1/2} - V_{i,j}^{k+1/2}],$$

where k is the index for time discretization, i for x-axis discretization, and j for z-axis discretization. dt is the grid step in time. dx and dz are the grid steps for the x-axis and for the z-axis, respectively, which are equal in these applications. Numerical velocity V at time $[k + 1/2]dt$, and numerical stress $(\Sigma, T) = (\sigma_{xy}, \sigma_{zy})$ at time kdt are computed explicitly from velocity at time $[k - 1/2]dt$ and stress at time kdt. L represents the lightness inside the medium and M the shear modulus. I emphasize the fact that each component of stress has its corresponding value of M, allowing a possible extension of this method to anisotropic media.

QUARTER-PLANE PROBLEM

The quarter-plane problem is a particular case of the infinite-wedge problem where the angle ϕ between the two edges is 90 degrees. As underlined by Wait (1959, p. 13), the solution can be found by image theory. A source S inside the medium induces three virtual image sources, as shown in Figure 2. Two images S_x and S_z are symmetric with respect to the real source along the x-axis and z-axis edges. The third image S_c is symmetric of the real source with respect to the corner. For a point source $S(x_s, z_s)$ with a time function $f(t_s)$, one can write the solution at the point $M(x, z)$ as

$$G(x, z, t; x_s, z_s, t_s) * f(t_s) \quad \text{incident wave,}$$

$$\pm G(x, z, t; -x_s, z_s, t_s) * f(t_s) \quad \text{edge reflection,}$$

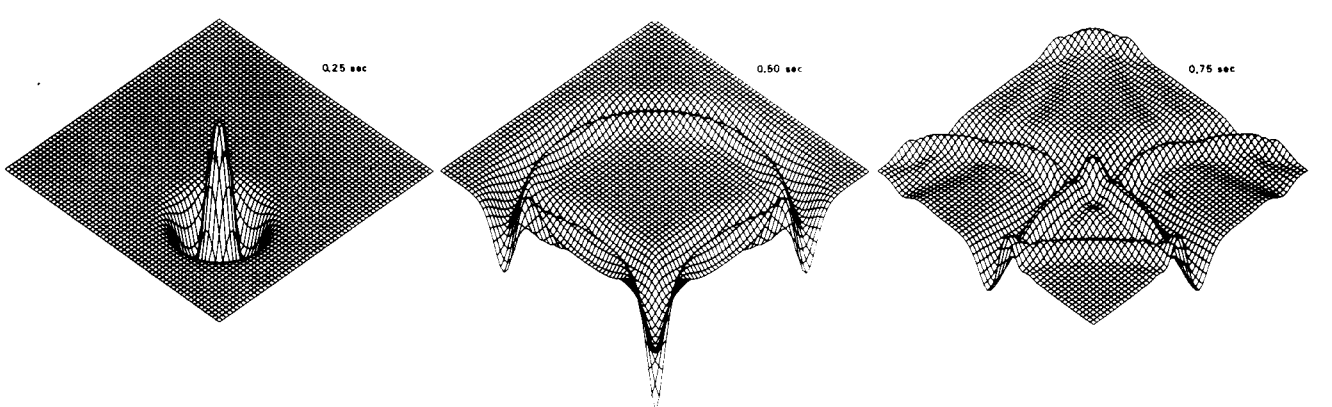

FIG. 3. Block diagram representation of quarter-plane problem for free edges at different times.

Table 1. Quarter-plane parameters.

Physical parameters	
Velocity	Source
3 000 m/s	$t_0 = 0.20$ s $\alpha = 1\,000$ (half-wavelength = 300 m)
Source position	Observer position
615 × 615 m^2	255 × 615 m^2
Numerical parameters	
$dx = 30$ m, $dt = 1.25$E-3 s, grid of 60 × 60 points	

$$\pm\, G(x, z, t; x_s, -z_s, t_s) * f(t_s) \qquad \text{edge reflection,}$$

and

$$+\, G(x, z, t; -x_s, -z_s, t_s) * f(t_s) \quad \text{corner reflection,}$$

where $G(x, z, t; x_s, z_s, t_s)$ is the Green's function for the infinite medium given as $H(t - r/c)/\sqrt{t^2 - r^2/c^2}$ with $r^2 = (x - x_s)^2 + (z - z_s)^2$ and c the velocity which can be found in Morse and Feshbach (1953, p. 842). For free boundary conditions on the two edges, S_x, S_z, and S_c are in-phase with S. However, for rigid boundary conditions on the two edges, S_x and S_z are in opposite phase with S, while S_c is still in-phase with S. Waves emitted by S_c represent the constructive interference of waves emitted by S_x and S_z. This so-called corner wave is always in-phase with the incident wave.

This problem is solved by employing the previously described numerical method. Table 1 gives the physical parameters of the problem. The usual rule of using at least ten grid points for the shortest wavelength of the source is respected for this scheme, as it should be for any second-order scheme (Alford et al., 1974). The finite size of the grid introduces two extra boundaries where radiation conditions are applied.

Results are depicted in a block diagram representation of the finite numerical grid at successive instants of time. Figure 3 concerns free edges. The first picture shows the incident solution in an infinite medium with a negative-positive pulse. The second picture shows the two in-phase reflections by the boundaries of the quarter-plane. Two parasite reflections from the absorbing boundaries may be observed, although they are weak. The third illustration adds the always in-phase corner reflection. Figure 4 concerns rigid edges. The only change from Figure 3 is the opposite phase of the reflections against boundaries.

Seismograms at a given point (Table 1) show more quantitatively the accuracy of the numerical solution by comparison with the analytical solution, given above. For free edges, Figure 5 depicts the three reflected pulses in-phase with the incident pulse, coming from the three images of the source. For rigid edges, on the other hand, Figure 6 depicts two reflected pulses out-of-phase with the incident pulse and one reflected pulse in-phase with the incident wave, which is the corner wave.

As proposed by Smith (1974), eliminating parasite reflections would have required solving four times the quarter-plane problem with a different set of boundary conditions (Neumann or Dirichlet conditions on the absorbing boundaries).

SEDIMENTARY BASIN AMPLIFICATION

Among a number of models of heterogeneous media, one has emerged as a sort of canonical example, solved by different numerical techniques. This model is a soft sedimentary basin lying on a half-space proposed by Aki and Larner (1970). The interface has the following equation:

$$z(x) = D + C/2\{1 - \cos\,[2\pi(x - w/2)/w]\}, \quad \text{for } -w/2 < x < w/2,$$

and

$$z(x) = D \qquad \text{elsewhere,}$$

where $w = 50$ km, $D = 1$ km, and $C = 5$ km. Sediments have a density $\rho_s = 2.0$ g/cm^3 and a velocity $v_s = 0.7$ km/s. The half-space has a density $\rho = 3.3$ g/cm^3 and a velocity $v = 3.5$ km/s.

An incident SH plane wave impinges normally from the

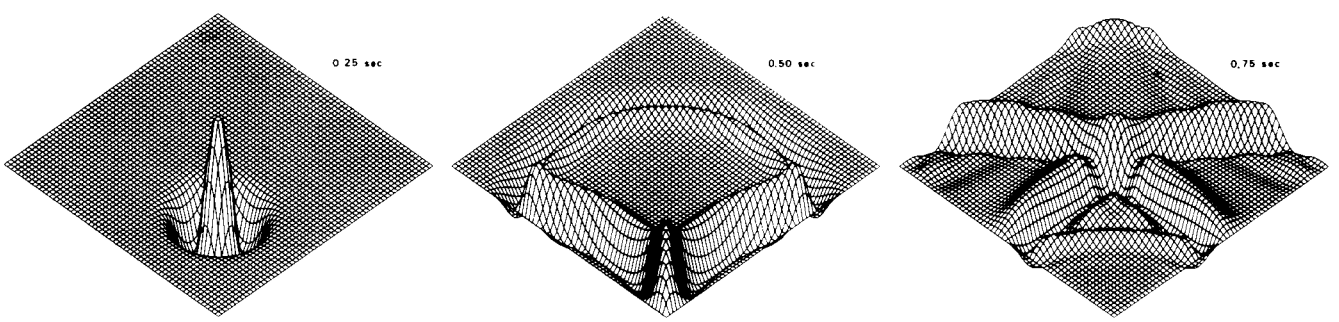

FIG. 4. Block diagram representation of quarter-plane problem for rigid edges at different times.

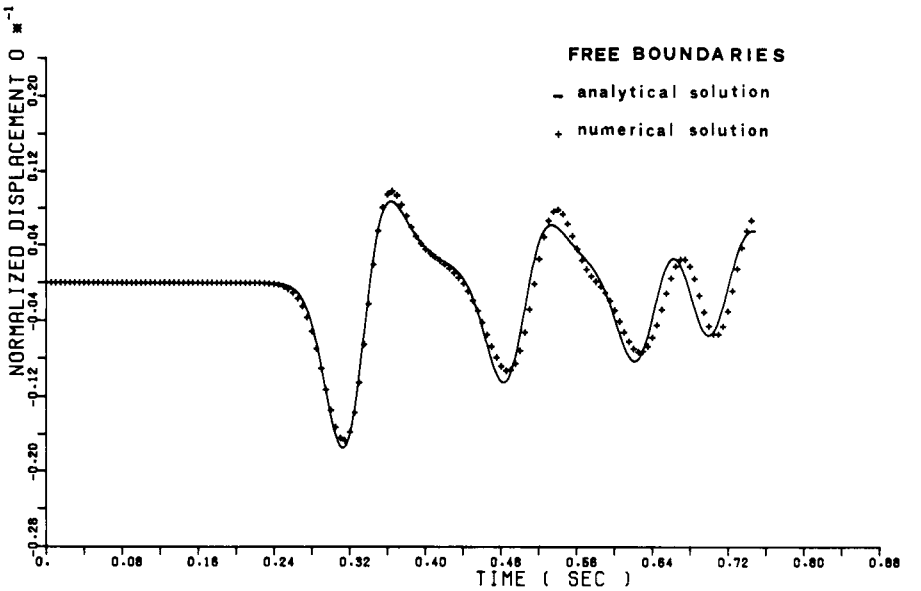

FIG. 5. Seismogram at a given observer (Table 1) for free edges. Note the three in-phase reflections.

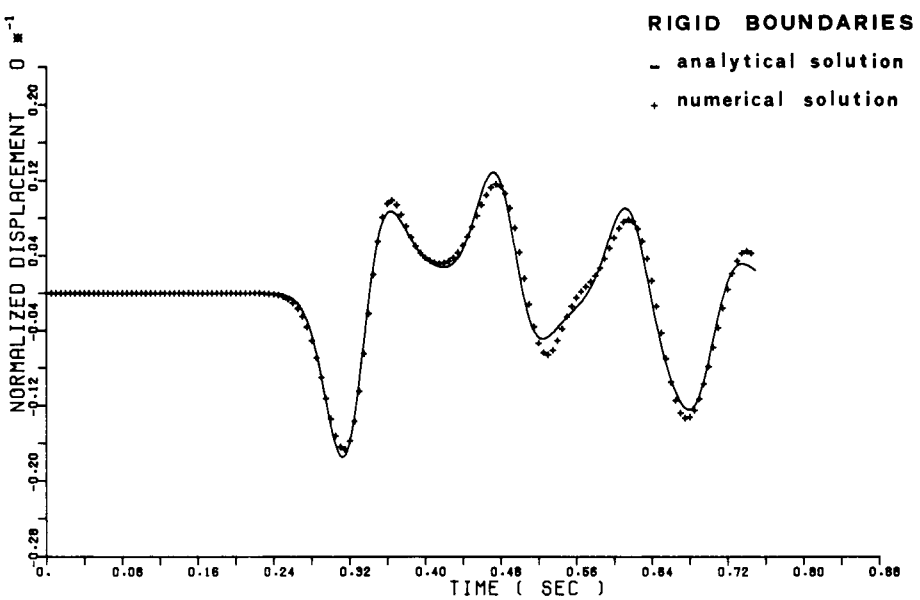

FIG. 6. Seismogram at a given observer (Table 1) for rigid edges. Note the two opposite phase reflections and the in-phase corner reflection.

half-space. Its source function is a Ricker wavelet, which is defined in a preceding paragraph, with $t_s = 20$ s and $t_p = 18.3$ s. In order to model correctly this plane wave, zero-stress conditions (equivalent to symmetric conditions) are applied to the two vertical boundaries. A radiative condition is chosen for simulating the half-space. The free surface of the earth ends the description of boundary conditions. The incident wave is applied just beneath the basin. Because reflections are nearly vertical, parasite reflections from the lateral boundaries are drastically diminished, enabling us to compute seismograms over a long period of time, in spite of the very high contrast in velocities.

Six seismograms are depicted in Figure 7, starting from the center of the basin with a step of 4 km. Five traces represent each station. The first seismogram was obtained by glorified optics (GO) (Hong and Helmberger, 1978). The second one is the result of finite-element calculation (FE) (see Hong and Helmberger, 1978). The third graph results from the Aki-Larner method (AL) (Bard and Bouchon, 1980). The fourth seismogram is an application of principal curvature (PC) (Lee and Langston, 1983), and the fifth one is the result of my finite-difference method (FD).

Good overall agreement is obtained, although the FE and FD methods are essentially long-period techniques while the GO, PC, and AL approaches are high-frequency approximations. A remarkable fit is observed between my result and the AL trace. FD reflections arrive a little earlier than the AL reflections but with the same waveform. This slight shift in time is due to the spatial discretization choice ($dx = 150$ m). A better agreement would have been observed with a finer grid.

This comparison between quite different techniques gives confidence in the accuracy of the implicit description of internal boundaries in FD method. Consequently, I turn attention toward a more difficult problem.

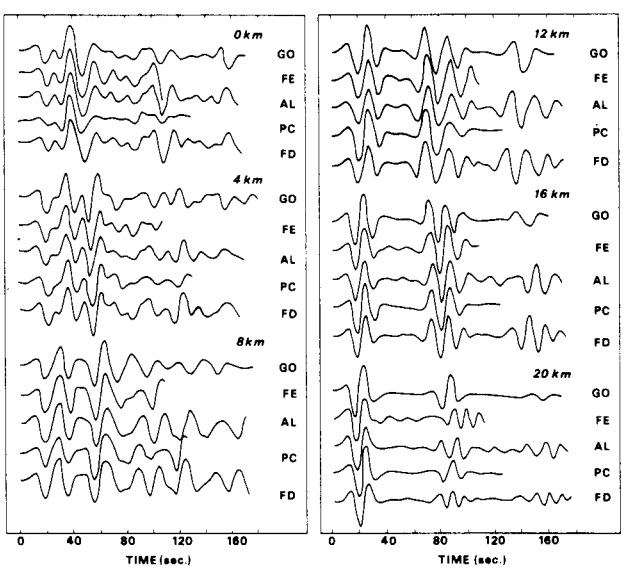

FIG. 7. Seismograms at six different positions over a sedimentary basin. Five traces are compared, coming from different methods.

SALT DOME: CORNER WAVE AND HEAD WAVE

Because of their time-space domain resolution, FD methods are designed for solving wave propagation in heterogeneous media where very abrupt changes occur in the interfaces (a fault, for example). Alford et al. (1974) and Kelly et al. (1976) studied corner diffractions. I intend to obtain seismic profiles over a rather simplified salt dome, and interpret strong reflected and diffracted phases.

The medium is composed of two layers. A dome rising from the lower medium intrudes the upper medium. The velocities are 2 500 m/s for the top layer and 4 500 m/s for the bottom layer. The precise geometry is shown in Figure 8. The distance between the horizontal interface and the free surface of the Earth is slightly larger than twice the distance between the top of the dome and the free surface. Therefore, two different waves arrive nearly on the same reflection hyperbola.

This rather simplified geometry is a combination of a quarter-plane problem and a 270 degree wedge problem. The first problem implies only reflections, while the second one induces diffraction. Tolstoy (1973, chap. 8) decomposed, for any angle ϕ of the wedge, the scattered field into a reflected part explained by image theory, plus a diffracted part emitted by the apex of the wedge. The second part vanishes for the quarter-plane problem. I use this interpretation in sketching wavefronts at different times.

The source is the impulsive point source of Alford et al. (1974) which I provided above. Its main advantage is a pulse of rather short time possessing a negative part and then a positive part, which is especially suited for identifying wavefronts in block diagrams. Three different shooting points on the Earth's surface illuminate the vertical wall of the dome, inducing lateral propagation in which I am interested. Radiation conditions are applied on the two vertical boundaries and on the lower horizontal boundary.

By choosing physical parameters of the lower medium, three different conditions can be studied at the interface between the two layers: free interface (stresses set to zero), rigid interface (velocities set to zero), and real interface (velocity contrast of 2 500 m/s over 4 500 m/s). Seismic profiles are shown over 8 km with 4 s of duration. The left end is chosen as the origin for measuring horizontal offsets.

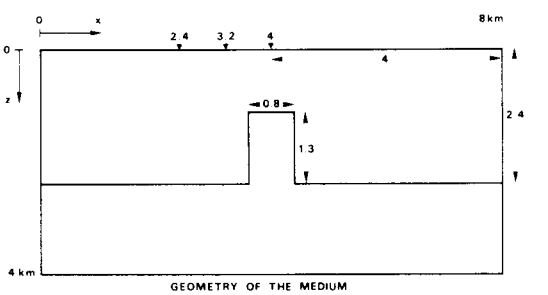

FIG. 8. Geometry of salt dome taken by finite-difference modeling.

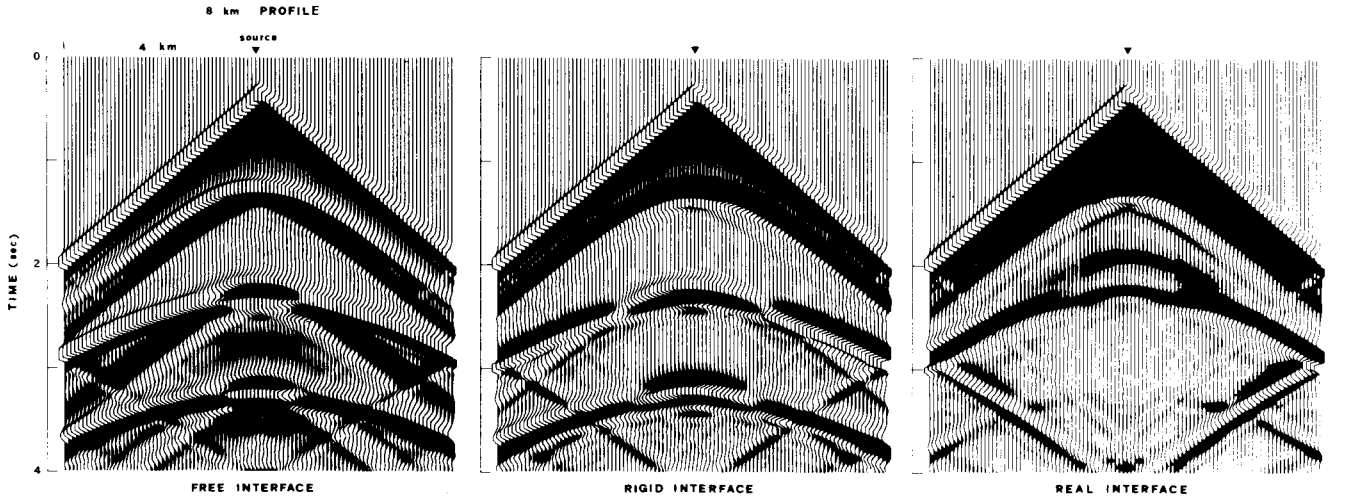

FIG. 9. Seismic profile for a source above the dome with a horizontal offset of 4 km.

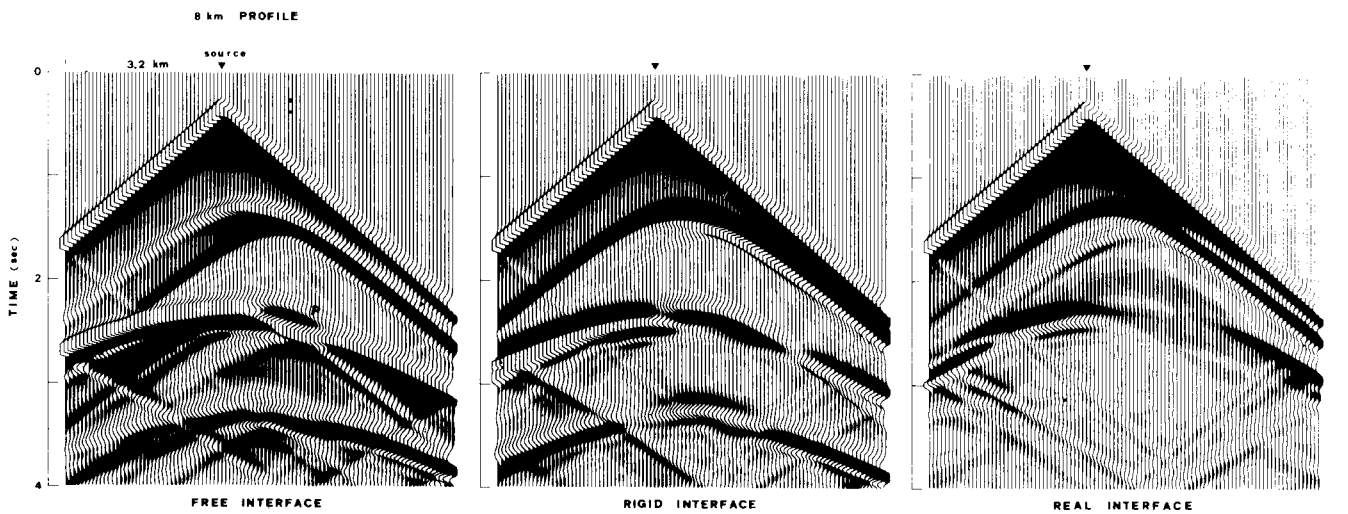

FIG. 10. Seismic profile for a source with a horizontal offset of 3.2 km.

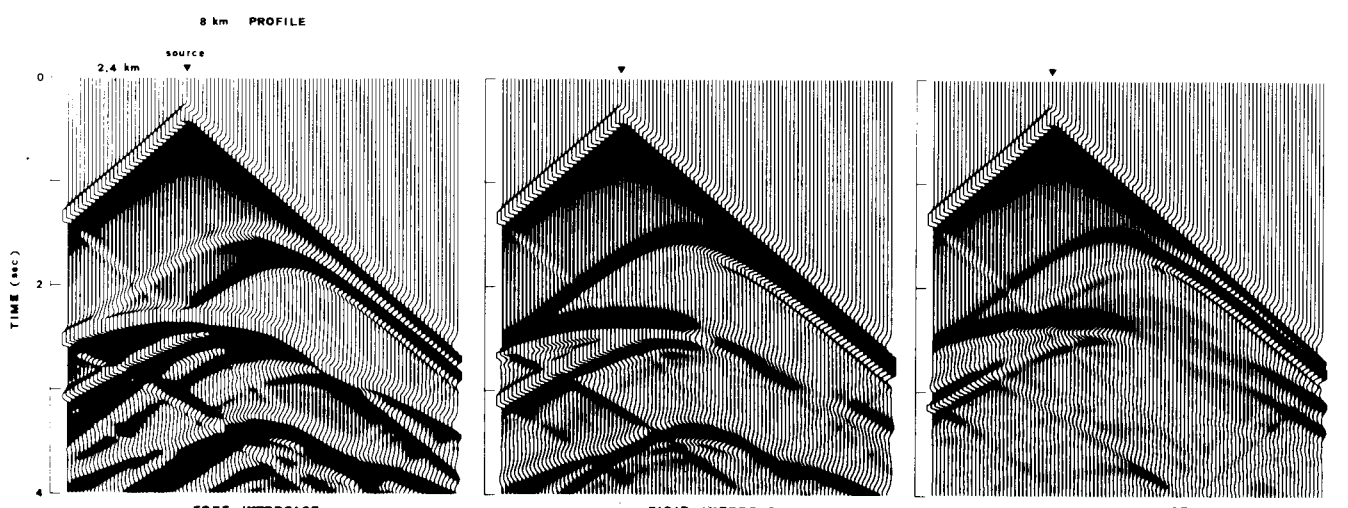

FIG. 11. Seismic profile for a source with a horizontal offset of 2.4 km.

Presenting the result for this FD simulation or other examples of complex wave propagation requires special graphic representation methods. I have used three. The first method incorporates standard seismic profiles, which are presented in Figures 9, 10, and 11. A saturation of the signal (set to 1/20) is used; this means that the maximum and minimum values are divided by 20 before plotting. Weak signals can be visualized in this way. The second method is a raster or point representation on a 512 × 512 screen using a gray table. The advantage is that of showing, with equal importance, the positive (white) and negative (black) parts of the signal as they depart from the zero (gray) level, while the standard representation emphasizes the negative part (black) of the signal. The third one is a movie (over 1 000 pictures for a 2 s duration) which enables one to follow the different wavefronts as they propagate. The importance of these representations for interpreting seismic profiles must be emphasized. I do not intend to explain in the following paragraphs every phase that was observed, but rather, I intend to emphasize those that are strong or characteristic of lateral propagation.

4 km source: Symmetric case

Figure 9 depicts the case where the source is just above the dome, with a horizontal offset of 4 km; in this case, the seismic profiles are symmetric. Following the incident wave, which has a reversed "V" shape, three sets of arrivals can be observed. In my interpretation, parasite reflections, which can easily be seen on pictures, will not be taken into account. I give a letter to upward fronts which are expected to be recorded at the Earth's surface.

Free interface.—The first profile is characterized by reflections in-phase with the incident wave. I show different phases arriving at the Earth's surface in Figure 12, and I interpret them with the help of diagrams of the medium showing wavefronts arriving at different times (Figures 13 and 14).

The first set of arrivals consists of the primary reflection at the top of the dome and primary diffractions by the upper corners of the dome. In the forward direction with respect to the corner, the diffraction, called phase A, is in-phase with the incident wave. In the backward direction, the diffraction, called phase B, is in opposite phase with the incident wave. This phase shifting has been explained by Tolstoy (1973, chap. 8). In Figure 13, I sketch these different waves.

The second set of arrivals which contains a first group of multiples shows an even more complex pattern. The phase A is again reflected by the top of the dome, giving the phase C, which is strong just above the dome. Behind this phase, the reflection, called phase D, of the incident wave on the horizontal interface arrives at the Earth's surface. Masked by this phase, the reflection of the phase A, called phase D, is missed, except maybe at the edges of the profile. The phase B is also reflected by the horizontal interface, giving the phase E with its specific black signature. The diffraction of the phase D on the upper corners follows immediately. Figure 14 summarizes these different phases.

The third set of arrivals contains mainly the reflection of the phase C, which is the double reflection of the phase A on the

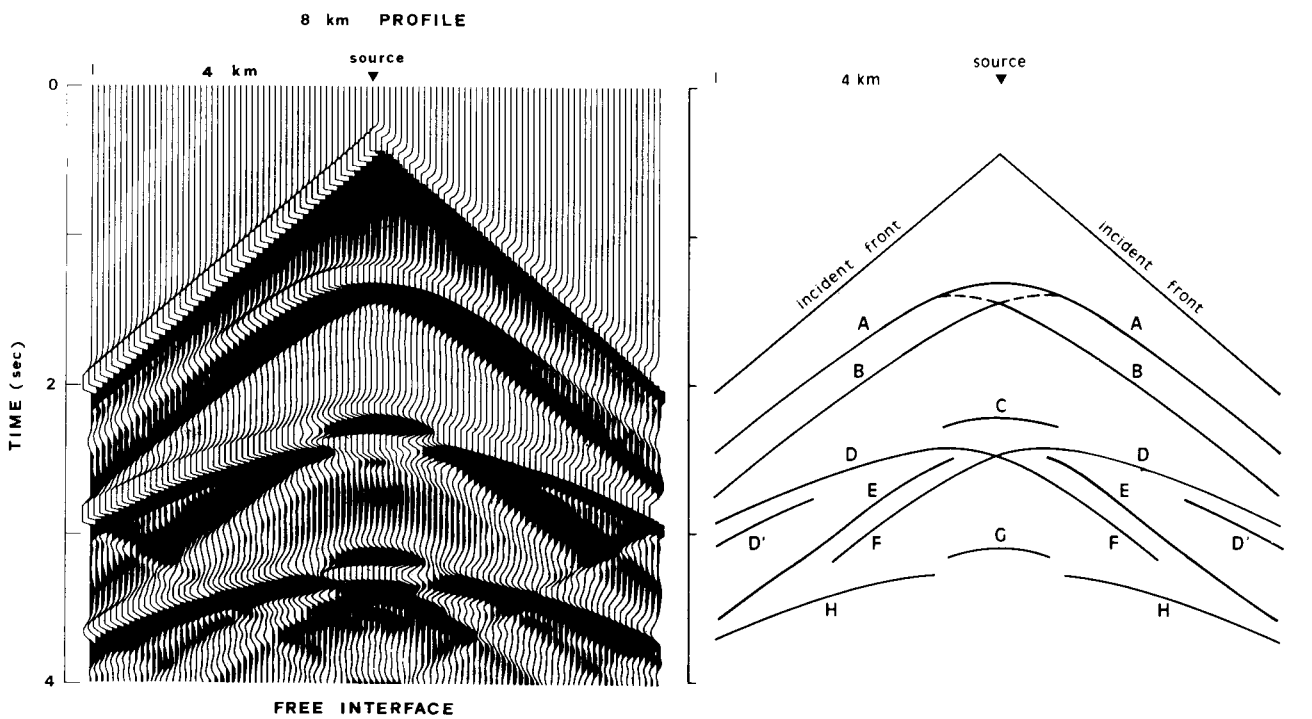

FIG. 12. Analysis of the free-interface profile is given in terms of the phases A, B, C, D, D', E, and F.

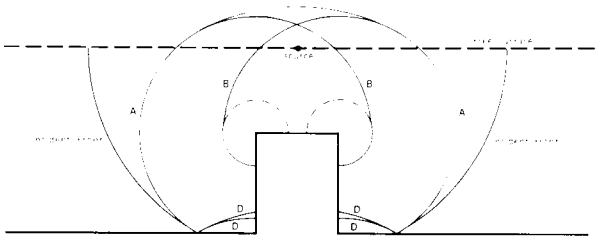

FIG. 13. Schematic interpretation of primary reflected and diffracted wavefronts. The free surface, in discontinuous line, does not reflect these phases in this figure.

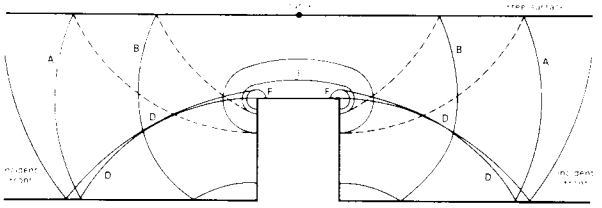

FIG. 14. Schematic interpretation of multireflected and diffracted wavefronts.

top of the dome, and the reflection of the phase B on the horizontal interface, after being reflected by the free surface. This concludes our description of the free-interface symmetric profile, which will be the frame for explaining the other profiles.

Rigid interface.—The second profile is characterized by reflections in opposite phase with the incident wave. The interpretation is analog to the free-interface one, taking into account the phase shifting of reflections. Of course, double reflections on the interface will again be in-phase with the incident wave. The only difference is a rather weak phase B, due to a phase shift. Its interpretation is left to a subsequent paragraph.

Real interface.—The third profile is characterized by weaker opposite phase reflections than previous ones. Part of the energy is carried away by the refracted wave, producing these weaker reflections, which can still be observed. No precise interpretation is given here, because the features of interest are not developed in this symmetrical case.

3.2 km source: Intermediate case

Figure 10 depicts profiles where the source is beginning to illuminate one of the two vertical walls of the dome. This figure provides a transition to the more asymmetrical case where lateral propagation features are well developed.

2.4 km source: Asymmetrical case

Figure 11 exhibits profiles where the source illuminates a vertical wall of the dome, inducing a lateral propagation that must be seen, somehow, at the surface of the Earth. Three sets of energy are still observed, after the incident wave. Depending upon which side of the dome the observer and the source are on, reflected waves will be strongly asymmetrical.

Free interface.—This profile presents strong lateral propagation features. The first set contains phases A and B, with their typical signatures. Horizontal offsets are due to the relative position of the source and the top of the dome.

In the second set, phase C is observed again with an increasing horizontal offset, thereby diminishing drastically the energy twice reflected on the top of the dome. Phase D, a reflection of the incident wave on the horizontal interface, is observed mainly on the side of the dome where the source is located, still masking the phase D′. Phase B which belongs to the first set, slightly perturbates phase D. The constructive interference between phase A and phase D gives the corner wave, which arrives after phase D, and with a rather steep slope. This corner wave, already observed in the quarter-plane problem, is a typical feature of lateral propagation and is only observed on the illuminated side of the dome. Just behind it, phase E writes its specific signature twice, depending on the concerned upper corner. Phase F is too weak to be observed.

Finally, in the third set, the reflection of phase C is outside the profile. The first reflection is simply the reflection of phase D on the top of the dome.

Rigid interface.—Two features must be emphasized in this profile.

In the first set, the weakness of phase B is explained this way: the source and the nearest diffracting upper corner play opposite roles because they diffract out-of-phase at the other corner. For the free interface, roles were added.

The second set shows that the corner wave is in-phase with the incident wave, while phases A and D are out-of-phase. This typical feature of the corner wave was already pointed out for the quarter-plane problem.

Real interface.—Similar features are observed, as for the rigid interface, but with a striking difference. A very strong wave arrives before the corner wave, which is not observed for free or rigid interfaces. This wave is a head wave for the diffracted wave from the lower corner of the dome, and is in-phase with

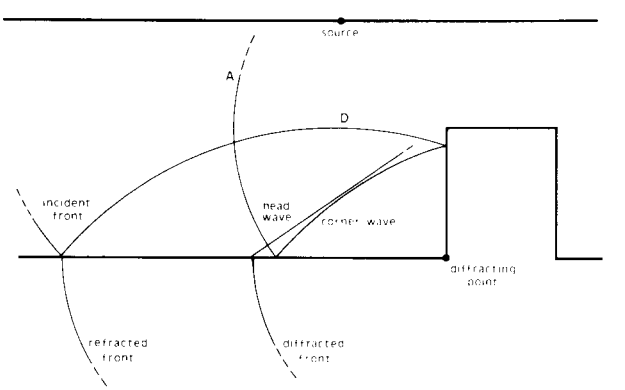

FIG. 15. Constructive interference of phases A and D gives the corner wave. For a real medium, the lower diffracting point develops a head wave in front of the corner wave.

the incident wave. It also partially overlaps the corner wave. Figure 15 sketches this head wave in front of the corner wave.

A partial conclusion is that lateral propagation stemming from the geometry of the medium implies two kinds of waves: the corner wave and the head wave, both inside the range of horizontal offsets for a reflection profile. Of course, these waves would have been less developed for a more complex geometry.

CONCLUSION

A numerical method, belonging to the heterogeneous formulation of finite-difference techniques, was presented for modeling *SH*-wave propagation in heterogeneous media.

This method solves the elastodynamic equations in terms of velocity and stress. It provides a symmetrical role to the lightness (inverse of density) and to the shear modulus. These quantities are naturally discretized where velocity and stress are discretized. Stress can be removed, but the shear modulus discretization must be kept as proposed in this paper. Therefore, modeling free, rigid, and real interfaces does not lead to any numerical transition zones.

Analysis of numerical results has been possible, only because powerful graphic tools were used for data interpretation; these include instantaneous raster representation of the medium with an immediate choice of the image saturation, and a very helpful movie. The profiles were analyzed by checking phases arriving at the surface of the Earth on the instantaneous raster representation or on the movie. The interpretation of profiles calculated for more complex media would have been impossible without these graphic tools.

This same method was used by Virieux and Madariaga (1982) for homogeneous *P/SV*-wave propagation (in-plane crack) and for homogeneous 3-D wave propagation (3-D crack). From this heterogeneous *SH*-wave propagation modeling procedure, extension for heterogeneous *P/SV* and 3-D wave propagation modeling should not present difficulties.

Interpreting reflection profiles is increasingly difficult, when lateral propagation becomes significant. Two kinds of waves, corner and head waves, appear which are very difficult to interpret with respect to horizontal stratigraphy.

ACKNOWLEDGMENTS

This work was supported by ATP "Géophysique appliquée à la prospection" and by ATP "Cray-Recherche." Dr. R. Madariaga critically reviewed this paper. We thank two unknown reviewers for their helpful comments.

REFERENCES

Aki, K., and Larner, K. L., 1970, Surface motion of a layered medium having an irregular interface due to incident plane *SH* waves: J. Geophys. Res., **75**, 933–954.

Aki, K., and Richards, P. G., 1980, Quantitative seismology, 1980: W. H. Freeman and Company.

Alford, R. M., Kelly, K. R., and Boore, D. M., 1974, Accuracy of finite-difference modeling of the acoustic wave equation: Geophysics, **39**, 834–842.

Alterman, Z., and Karal, F. C., 1968, Propagation of elastic waves in layered media by finite-difference methods: Bull., Seism. Soc. Am., **58**, 367–398.

Bard, P. Y., and Bouchon, M., 1980, The seismic response of sediment-filled valleys. Part 1: The case of incident *SH* waves: Bull. Seism. Soc. Am., **70**, 1263–1286.

Boore, D. M., 1972, Finite-difference methods for seismic wave propagation in heterogeneous materials, *in* Methods in computational physics, **11**: B. A. Bolt, ed., Academic Press, Inc.

Clayton, R. W., and Engquist, B., 1980, Absorbing boundary conditions for wave-equation migration: Geophysics, **45**, 895–904.

Červeny, V., Molotkov, I. A., and Psencik, I., 1977, Ray method in Seismology: Univ. Karlova, Praha.

Hong, T. L., and Helmberger, D. V., 1978, Glorified optics and wave propagation in nonplanar structure: Bull. Seism. Soc. Am., **68**, 2013–2032.

Kelly, K. R., Ward, R. W., Treitel, S., and Alford, R. M., 1976, Synthetic seismograms: A finite-difference approach: Geophysics, **41**, 2–27.

Kummer, B., and Behle, A., 1982, Second-order finite-difference modeling of SH-wave propagation in laterally inhomogeneous media: Bull., Seism. Soc. Am., **72**, 793–808.

Lee, J. J., and Langston, C. A., 1983, Three-dimensional ray tracing and the method of principal curvature for geometric spreading: Bull. Seism. Soc. Am., **73**, 765–780.

Madariaga, R., 1976, Dynamics of an expanding circular fault: Bull., Seism. Soc. Am., **65**, 163–182.

Mitchell, A. R., 1969, Computational methods in partial differential equations: John Wiley and Sons.

Morse, P. M., and Feshbach, H., 1953, Methods of theoretical physics: McGraw-Hill Book Co., Inc.

Sanchez-Sesma, F. J., and Esquivel, I. A., 1979, Ground motion on alluvial valleys under incident plane *SH* waves: Bull. Seism. Soc. Am., **69**, 1107–1120.

Smith, W. D., 1975, The application of finite-element analysis to body wave propagation problems: Geophys. J. Roy. Astr. Soc., **42**, 747–768.

Smith, W. D., 1974, A nonreflecting plane boundary for wave propagation problems: J. Comp. Phys., **15**, 492–503.

Tolstoy, I., 1973, Wave propagation: McGraw-Hill Book Co. Inc.

Virieux, J., and Madariaga, R., 1982, Dynamic faulting studied by a finite difference method: Bull., Seism. Soc. Am., **72**, 345–369.

Wait, J. R., 1959, Electro-magnetic radiation from cylindrical structures: Pergamon Press Inc.